Chemical Science

ROYAL SOCIETY OF CHEMISTRY

EDGE ARTICLE

View Article Online
View Journal | View Issue

Cite this: *Chem. Sci.*, 2022, **13**, 5964

All publication charges for this article have been paid for by the Royal Society of Chemistry

A visible light/heat responsive covalent organic framework for highly efficient and switchable proton conductivity†

Yongkui Chen,[ab] Jikuan Qiu,[a] Xia-Guang Zhang,[a] Huiyong Wang,[a] Wenhui Yao,[b] Zhiyong Li,[a] Qingchun Xia,[a] Guangshan Zhu*[c] and Jianji Wang *[a]

Received 13th April 2022
Accepted 26th April 2022

DOI: 10.1039/d2sc02100e

rsc.li/chemical-science

In recent years, covalent organic frameworks (COFs) have attracted enormous interest as a new generation of proton-exchange membranes, chemical sensors and electronic devices. However, to design high proton conductivity COFs, especially those with stimulus responsive performance remains a great challenge. Here, the first example of a light/heat switchable COF (**COF-HNU9**) has been synthesized by grafting a donor–acceptor Stenhouse adduct (DASA) within the channels of a β-ketoenamine-based COF. DASA groups in the nanopores of **COF-HNU9** undergo a reversible open–closed photoisomerization upon visible light irradiation and are recovered by heating. Thus, **COF-HNU9** exhibits not only a remarkably high proton conductivity, but also a highly effective switching performance. Under visible light irradiation at 98% RH, the proton conductivity of **COF-HNU9** increases by three orders of magnitude at 25 °C and is up to 0.02 S cm^{-1} at 80 °C. Furthermore, the proton conductivity does not display any significant decrease even after 20 switching cycles. These results have been rationalized by a Grotthuss-type mechanism and verified by DFT calculations. The stimuli-responsive COF is conceptually confirmed by an optical control device with the light/heat switching proton conductive **COF-HNU9** film, which is able to remote-control the illumination and switching off of an LED lamp without any current amplifier.

Introduction

Proton exchange membrane (PEM) fuel cells[1,2] and electronic devices[3–5] have advantages such as high power density, zero pollution, and mild working conditions, therefore they have attracted extensive attention in recent years. The proton-conductive material for the PEM is the key component of these devices. From the viewpoint of practical application, a promising candidate for solid state proton conductors requires not only high proton conductivity but also high stability to make them viable for long-term performance.[1c] At present, many solid proton electrolytes are mainly based on polymeric materials, particularly perfluorosulfonic polymers due to their high proton conductivity.[2b] Nonetheless, the amorphous nature of these polymers makes it difficult to regulate the transport pathway of protons and then to improve the proton conductivity. Thus, great efforts have been devoted to developing new stable proton conductors with well-defined pore structures, high proton conductivity and tunability.[6–9]

Covalent organic frameworks (COFs) are a new class of crystalline polymers covalently constructed from organic building blocks.[10] Due to the unique characteristics of periodic structure, designable regular open channels, and tunable functionality, COFs offer a useful platform for exploring new proton conductors[11–14] and have shown great potential in PEM fuel cells and electronic devices.[15–19] For example, two novel sulfonated COFs were designed and synthesized by Zhao and co-workers,[12] and both of these COFs showed high intrinsic proton conductivity of up to 3.96×10^{-2} S cm^{-1} at 97% relative humidity (RH) under ambient conditions because of the denser content of sulfonic acid groups. Banerjee's group[15a] reported the first example of an extrinsic proton-conducting COF (**Tp–Azo**) synthesized from triformylphloroglucinol (**Tp**) and 4,4′-azodianiline (**Azo**), where H_3PO_4 was immobilized in **Tp–Azo** and applied as a proton conductor to obtain a conductivity of 9.9×10^{-4} S cm^{-1} at 59 °C and 98% RH. Recently, Zhu's group[16a] prepared a cationic COF and then the phosphotungstic anionic $PW_{12}O_{40}^{3-}$ was introduced by ion exchange for proton

[a]*Collaborative Innovation Center of Henan Province for Green Manufacturing of Fine Chemicals, School of Chemistry and Chemical Engineering, Key Laboratory of Green Chemical Media and Reactions, Ministry of Education, Henan Normal University, Xinxiang, Henan 453007, P. R. China. E-mail: jwang@htu.edu.cn*

[b]*School of Chemistry and Materials Engineering, Xinxiang University, Xinxiang, Henan, 453003, P. R. China*

[c]*Key Laboratory of Polyoxometalate and Reticular Material Chemistry of Ministry of Education, Faculty of Chemistry, Northeast Normal University, Changchun 130024, P. R. China. E-mail: zhugs@nenu.edu.cn*

† Electronic supplementary information (ESI) available: Materials and instrumentation methods, synthetic procedures, Nyquist plots under ideal conditions, FT-IR spectra, SEM and TEM images, BET plots, TGA analysis, PXRD patterns, XPS spectra, UV-vis spectra, stability test, water vapor sorption isotherms and proton conductivity measurement. See https://doi.org/10.1039/d2sc02100e

conduction, and the charged COF exhibited a proton conductivity of 3.32×10^{-3} S cm^{-1} at room temperature and 97% RH. In another example, Jiang and co-workers[17a] reported an ultrastable COF in which H_3PO_4 was confined for efficient proton conduction at high temperature. The anhydrous proton conductivity was high up to 1.91×10^{-1} S cm^{-1} at 160 °C upon continuous running over 20 h. However, literature survey reveals that stimuli-responsive proton conductive COFs have never been reported so far in spite of their great potential in remote-controllable sensors and electronic devices as shown by stimuli-responsive metal organic frameworks (MOFs).[20,21]

Among various external stimuli,[22] visible light is one of the most appealing, widely available, and environmentally friendly triggers.[23] Significantly, light signal can be controlled remotely and precisely in space and time and switched rapidly in a clean and noninvasive way.[24] For the fabrication of light-responsive porous materials, an attractive strategy is to incorporate photo-switchable molecules, including azobenzene, spiropyran and diarylethene,[25] into the modular framework structures. Recently, a new kind of light/heat switchable molecules, donor–acceptor Stenhouse adduct (DASA), has been reported, which is capable of a reversible switching between the open neutral state (DASA-O) and closed zwitterionic state (DASA-C) triggered by visible light irradiation and heating in non-polar aromatic solvents.[26] Such a structural transformation results in a significant dipole moment change of the molecules. Thus, DASA can be considered to be a promising candidate of photo-switchable molecules for light-responsive porous materials.

Herein, for the first time, DASA groups were incorporated within the channels of a β-ketoenamine-based COF as dangling groups by chemical grafting to form a photoresponsive smart COF (denoted as **COF-HNU9**). We found that the pendent DASA groups in **COF-HNU9** showed photoswitchable property from the open neutral state (**COF-HNU9-O**) to the closed zwitterionic state (**COF-HNU9-C**) under the irradiation of visible light and were recovered by heating, which is similar to the dissolved molecules in aromatic solvents. Importantly, the as-synthesized **COF-HNU9** exhibits three orders of magnitude increase in proton conductivity compared with the DASA-free β-ketoenamine-based COF after visible light irradiation at 25 °C and 98% RH when reaching the photostationary state, and the proton conductivity is as high as 0.02 S cm^{-1} at 80 °C. It is also revealed that the proton conductance in the light-responsive COF follows a Grotthuss-type mechanism. As a proof of concept, a light-controlled proton conductive film was assembled into a photo-responsive device to realize the switchable lighting and turning off of a light-emitting diode (LED) lamp without any current amplifier. It was clearly demonstrated that the device was able to illuminate the LED lamp under irradiation with visible light, which could then be switched off in the dark as shown in Fig. 1.

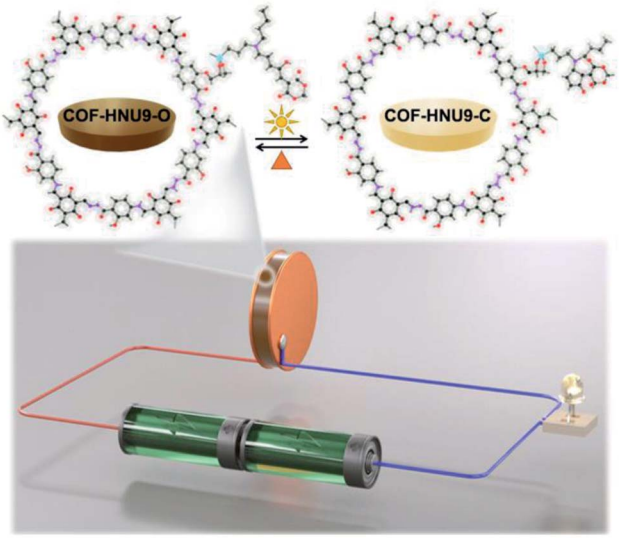

Fig. 1 Illustration of the photo-controlled circuit to light the LED lamp due to the change in proton conductivity resulting from the open–closed–open isomerization of DASA groups in **COF-HNU9** switched by visible light and heat.

Results and discussion

Due to the high chemical stability and easy derivative nature, in this work, we selected a β-ketoenamine-linked COF (**TpASH**) with free hydroxyl (−OH) groups as the parent framework for the synthesis of DASA functionalized COFs. **TpASH** was synthesized *via* a condensation reaction between 1,3,5-triformylphloroglucinol (**Tp**) and 4-aminosalicylhydrazide (**ASH**) by a traditional solvothermal approach (see details in the ESI†). Compared to the original synthetic route by solid grinding,[27] the **TpASH** synthesized by the solvothermal approach showed much enhanced crystallinity. The chemical structure of the **TpASH** is shown in Fig. 2a and characterized by FT-IR (Fig. S1†), SEM and TEM (Fig. S2†), and PXRD (Fig. 2b), which suggest the preferable crystal structure of the AA eclipsed stacking mode (Fig. 2c). It was found that **TpASH** had a BET surface area of 614 m^2 g^{-1} (Fig. S3†), which is obviously higher than that synthesized by solid grinding reported in the literature (500 m^2 g^{-1}).[27] The total pore volume of **TpASH** was estimated (at $P/P_0 = 0.99$) to be $V_p = 0.50$ cm^3 g^{-1} (Fig. S3†). Meanwhile, high thermal stability (Fig. S4†) and chemical stability (Fig. S5†) of the **TpASH** were also confirmed.

The visible light and heat responsive **COF-HNU9** was synthesized by anchoring the photo-switchable DASA molecules onto the channel walls using post-synthetic modification steps. Due to the high reactivity, moderate greasy nature, and suitable photostationary/dark equilibrium,[28] (3-butylaminopropyl)trimethoxysilane was chosen as the "donor" amine to react with activated furans to synthesize DASA units. It was noted that the FT-IR spectra of **COF-HNU9** exhibited asymmetric and symmetric C–H stretching vibration peaks at 2920 and 2853 cm^{-1}, respectively (Fig. S6†), confirming the existence of the methyl and methylene fragments of the linking groups. As shown by the PXRD patterns in Fig. 2b, **COF-HNU9** showed a similar diffraction pattern to that of **TpASH** but with a broadened peak width at $2\theta = \sim 4.0°$. This result can be ascribed to the existence of a large number of flexible chains in the cavities of **COF-HNU9**, thus slightly contorting the π–π

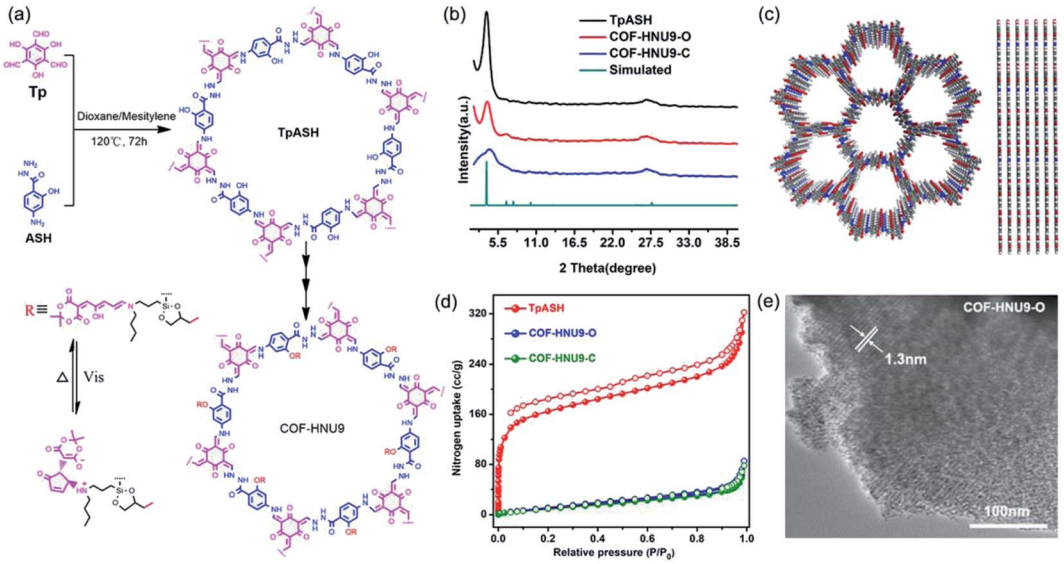

Fig. 2 (a) Synthetic scheme of **TpASH** and **COF-HNU9**. (b) PXRD patterns of **TpASH** and **COF-HNU9**. The first peak in the PXRD pattern is retained after post-synthetic modification signifying its structural integrity. (c) Views of the layered 2D-crystal structure of **TpASH** resulting from an eclipsed AA stacking model. (d) Nitrogen absorption curves of **TpASH** and **COF-HNU9** at 77 K. (e) TEM image of **COF-HNU9** before visible light irradiation.

stacking interactions between its layers. SEM analysis indicates that **COF-HNU9** had similar morphology to that of **TpASH** (Fig. S2†), but its BET surface area was only 54 $m^2\ g^{-1}$ (Fig. 2d). This low surface area compared to the DASA-free **TpASH** (614 $m^2\ g^{-1}$, Fig. S3†) could be caused by the presence of the DASA groups within the pores. The total pore volume of **COF-HNU9** was also estimated, which was about 0.13 $cm^3\ g^{-1}$. Such a significant decrease after DASA modification indicates once again that the DASA functional group is distributed inside the pores of **COF-HNU9** and occupies a certain pore volume. We also measured the CO_2 adsorption isotherm of **COF-HNU9** at 195 K, which showed a type I adsorption isotherm (Fig. S7†) and a BET surface area of 125 $m^2\ g^{-1}$ (Fig. S7†). It is clear that the BET surface area was much higher than that (54 $m^2\ g^{-1}$) determined by the N_2 adsorption isotherm of **COF-HNU9** at 77 K. This indicates that the flexible DASA units might block the pore opening at low temperatures like 77 K, whereas 195 K is a temperature that is high enough to give the DASA units sufficient flexibility and thus a higher value of BET surface area. The pore size distribution profiles revealed that **COF-HNU9** exhibited only one type of micropore structure with the size distribution at 1.3 nm (Fig. S8†), which is smaller than the value of 1.5 nm before functionalization (Fig. S3†). All these results were well consistent with that derived from HR-TEM analysis (Fig. 2e). In addition, compared with **TpASH**, the solid state ^{13}C NMR spectrum of **COF-HNU9** exhibited additional characteristic signals of $-CH_3$, $-CH_2$ and –CH of the DASA groups at around 6, 19–62, and 70 ppm, respectively (Fig. 3a and b), verifying the successful incorporation of DASAs in **TpASH** as dangling groups. The elemental analysis of **COF-HNU9** showed that the C, H, N, and O contents were 52.12, 6.33, 9.59 and 27.50%, respectively, which were close to the values of 57.69, 5.55, 7.92 and 24.87% estimated from an infinite 2D sheet ($C_{34}H_{39}N_4O_{11}Si$).

The isomerization of the DASA groups in **COF-HNU9** was investigated by various characterization techniques. As shown in Fig. 3b, two new peaks were observed at about 27 ppm and 203 ppm in the solid state ^{13}C NMR spectra of **COF-HNU9-O** compared to that of **COF-HNU9-C**, which correspond to C7′ and C11′ of the five-membered ring of the closed DASA groups. Meanwhile, the peak at about 50 ppm corresponding to the broadening of the C6′ peak was also observed because of the influence of the NH^+ cation. The appearance of these new peaks and peak broadening indicates that structural transformation happened from **COF-HNU9-O** into **COF-HNU9-C** after visible light irradiation (Fig. 3a). In the XPS spectrum before and after visible light irradiation (Fig. 3c and d), two N spectra and two O spectra were used directly without fitting to compare the structural changes. It is clearly noted that after visible light irradiation on the **COF-HNU9**, the binding energy of N 1s and O 1s significantly shifted from 401.7 and 531.9 eV to 400.9 and 531.3 eV, respectively (Fig. 3c and d). This result indicates that DASA groups in **COF-HNU9** were isomerized after visible light irradiation. In order to explore the changes in atom types before and after visible light irradiation, the core-level C 1s, N 1s and O 1s XPS spectra were deconvoluted into different peaks, respectively (Fig. S9†). The peaks at 400.3 eV (N 1s) and 532.5 eV (O 1s) can be assigned to C–N and C═C–OH (Fig. S9c and e†) in the structure of **COF-HNU9-O**.[29] After irradiation with visible light, they shifted to higher binding energies of 401.8 eV (N 1s) and 533.0 eV (O 1s), which correspond to $C–N^+$ and $C–O^-$ (Fig. S9d and f†), respectively.[30] These results were attributed to the photoisomerization of the DASA groups in the **COF-HNU9-C** pores. Furthermore, **COF-HNU9** showed different thermal decomposition temperatures of 200 and 120 °C before and after

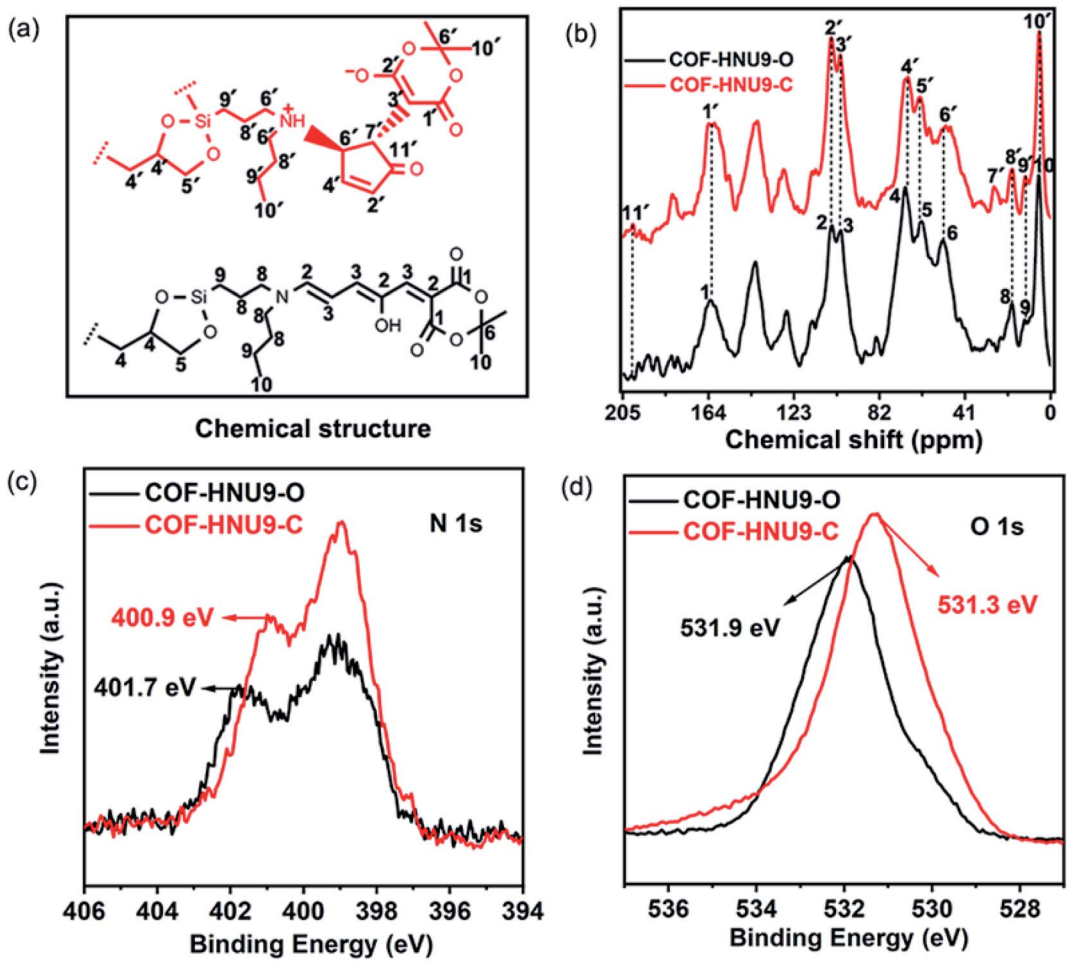

Fig. 3 (a) The structure and carbon atom numbering of DASA groups in the as-prepared **COF-HNU9-O** and **COF-HNU9-C**. (b) The ^{13}C CP MAS solid state NMR spectra of **COF-HNU9-O** and **COF-HNU9-C**. (c and d) Comparison of the XPS survey of N 1s spectra (c) and O 1s spectra (d) of **COF-HNU9** before and after visible light irradiation.

visible light irradiation (Fig. S4†). This result suggested that the open form was more thermally stable than the closed state, which probably resulted from the large conjugation and strong π–π interactions in the open structure of DASA groups. In addition, the loading value of the DASA moieties on **COF-HNU9** was calculated to be 0.44 ± 0.04 mmol g^{-1} from the thermogravimetric analysis results (Fig. S4†).

The isomerization was also studied by using UV-vis spectroscopy[31] and the results are presented in Fig. 4a. The intensity of the characteristic absorption band of **COF-HNU9-O** at 350–600 nm significantly decreased (see curves 1 and 2) under irradiation with 515 nm visible light, but recovered almost to the original intensity by heating (see curve 3). The conversion yield was found to be 65.3% (Fig. S10†) and 85.1% (Fig. S11†), respectively, after the isomerization equilibrium was achieved. This open–closed–open isomerization was switchable for many consecutive cycles without obvious photodegradation (Fig. S12†). In order to better illustrate the reversible isomerization of the DASA groups in **COF-HNU9**, we synthesized a small molecule DASA from (3-butylaminopropyl) trimethoxysilane and activated furans according to the procedures reported in the literature[26a] (see details in the ESI†). The photoisomerization of the molecules was monitored by UV/vis spectroscopy in ethyl acetate (Fig. S13†). It was found that the intensity of the absorption band centered at 538 nm decreased continuously upon irradiation with visible light. This change indicated that the small molecule DASA was significantly transformed into its colourless cyclopentenone isomer. The resulting solution was subsequently kept in the dark at room temperature. The absorption band almost went back to the original intensity due to the thermal reversion to the colored triene.[32] These results were well consistent with that of **COF-HNU9**.

The visible light and heat triggered reversible isomerization of the DASA groups in **COF-HNU9** was further supported by water contact angle measurements on a glass surface coated initially with the freshly prepared **COF-HNU9**. The surface coated with the open **COF-HNU9-O** was found to be hydrophobic in nature with a contact angle of 115 ± 1.0° (Fig. 4b). Then the open **COF-HNU9-O** was isomerized to the closed **COF-HNU9-C** after visible light irradiation, and the contact angle decreased to 82 ± 1.0° (Fig. 4c). Then, the contact angle was

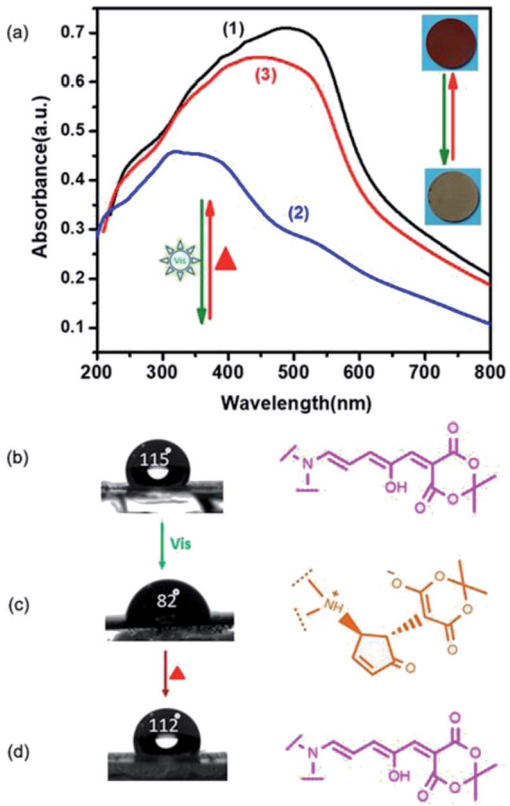

Fig. 4 (a) UV-vis spectrum change for the isomerization of COF-HNU9-O (1) to COF-HNU9-C (2) upon irradiation with a 515 nm light and for the recovery of the UV-vis spectra of COF-HNU9-O upon mild heating at 40 °C in the dark under 32% RH (3); (b–d) contact angle of a water droplet on a COF-HNU9-coated glass surface before and after visible light-irradiation and reversed by heating (corresponding to (1)–(3) in (a)).

restored to 112 ± 1.0° by mild heating at 40 °C in the dark under 32% RH (Fig. 4d and S14†), which was in good agreement with UV-vis results. The water vapor adsorption isotherm for **COF-HNU9** was also measured at 25 °C before and after irradiation with visible light. It was found that water adsorption capacity increased from 7.83 to 10.55 mmol g^{-1} under 97% RH, confirming that the hydrophilicity of **COF-HNU9** pores was enhanced after visible light irradiation (Fig. S15†).

We evaluated the proton conductivity of **COF-HNU9** by AC impedance spectroscopy using the compacted films with a thickness of 0.5 to 2 mm after saturating with water vapor for more than 3 h at different RH. As shown by our Nyquist plots (Fig. S16†), the proton conductivity of the **COF-HNU9** film in the dark (**COF-HNU9-O**) was 1.86×10^{-6} under 32% RH and 5.62×10^{-5} S cm^{-1} under 98% RH at 25 °C, which shows that increasing RH facilitates proton conductivity, but the hydrophobic framework of **COF-HNU9-O** cannot provide high conductivity even at a high RH (Fig. 5a). However, after visible light irradiation, the proton conductivity of **COF-HNU9-C** exhibited a significant increase with increasing RH and reached 3.74×10^{-3} S cm^{-1} at 98% RH and 25 °C (Fig. S16†), which is about 1000 times conductivity increment compared to the value (3.50×10^{-6} S cm^{-1}) of DASA-free **TpASH** under the same conditions. Therefore, both the isomerization of the grafted DASA groups and the high RH are of great importance in the significant enhancement of proton conduction.

In Fig. 5b, we studied the proton conductivity of **COF-HNU9** film before and after irradiation with visible light at 98% RH in the temperature range from 25 °C to 80 °C. It can be seen that the proton conductivity under visible light significantly increased from 3.74×10^{-3} to 0.02 S cm^{-1} when the temperature rose to 80 °C, showing that in addition to visible light irradiation and high RH, temperature was also an important factor that affected proton conductivity. Conventionally, AC impedance is composed of ohmic resistance, proton-transfer resistance and proton-diffusion resistance under ideal conditions (Scheme S4†).[33] Theoretically, visible light irradiation and high RH are greatly beneficial to the proton transport and diffusion, but to a different extent. This has been confirmed by our experimental Nyquist plots (Fig. S16†). Upon irradiation of visible light or increase of RH from 32% to 98%, the ohmic resistance and proton-transfer resistance became small and even disappeared at 25 °C (Fig. S16†). However, the proton-diffusion resistance still remained although its value was also obviously decreased. This indicates that the proton-diffusion resistance was mainly responsible for proton conduction in this case. On the other hand, the preferable crystal structure of the AA eclipsed stacking mode of **COF-HNU9** resulted in regular open channels; as a result, proton conduction happened conveniently not only in the regular interlayers of parallel crystal planes, but also in the channels of **COF-HNU9**. Thus, the effect of thicknesses (0.5–2 mm) of the films on the diffusion resistance of samples was greatly reduced and even negligible, as shown in Fig. 5c. This type of behavior was similarly observed by Yu and co-workers.[25b]

We determined the equilibrium time of conductivity for the transformation of DASA units from the open to the closed state in **COF-HNU9** upon visible light irradiation at 80 °C and 98% RH. It was found that the proton conductivity rapidly increased in the first 5 hours of irradiation, and then became almost constant when the transformation reached the photostationary state (Fig. S17†). We also evaluated proton transport number in the temperature range of 25 to 80 °C (see details in the ESI†),[34] and found that it was in the range of 0.82 to 0.98 (Fig. S18†), indicating that **COF-HNU9** is an excellent proton conductor. In addition, the reversible switching of proton conductivity was examined at 25 °C and 98% RH. Unless otherwise specified, it takes about 120 minutes from the open to closed isomers, and 180 minutes for its reverse, which is close to that of some azobenzene decorated COFs reported in the literature by using ultraviolet light as a trigger.[25d] It was shown that no significant decrease of the proton conductivity was observed even after 20 cycles (Fig. 5d), exhibiting excellent reversibility and recyclability.

Next, we analyzed the quantitative relationship between conductivity and temperature under visible light irradiation at 98% RH. As shown in Fig. 5e, the proton conduction of DASA-free **TpASH** and **COF-HNU9** films follows an Arrhenius-like behavior. The activation energy (E_a) of **TpASH** film was 0.44 eV, which was close to the value for the Grotthuss

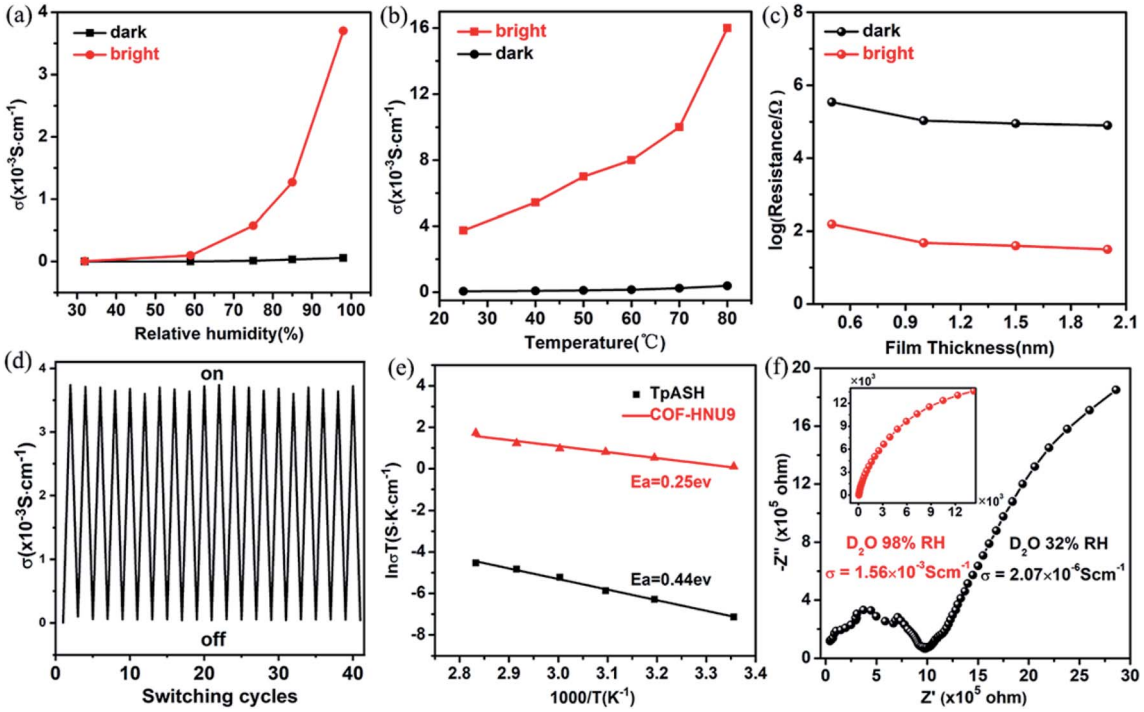

Fig. 5 (a) Proton conductivity of **COF-HNU9** film with increasing RH at 25 °C. (b) Proton conductivity of **COF-HNU9** film at 98% RH with the increase of temperature. (c) Resistance of the open and closed states of **COF-HNU9** with different film thicknesses (0.5, 1, 1.5 and 2 mm) before and after irradiation with visible light. (d) Reversible proton conductivity between 3.74×10^{-3} S cm^{-1} and 5.62×10^{-5} S cm^{-1} of **COF-HNU9** film by turning on/off light illumination at 25 °C and 98% RH. (e) Arrhenius plots of the **TpASH** and **COF-HNU9** films under visible light irradiation at 98% RH. (f) Nyquist plots of **COF-HNU9** film at 25 °C under 32% and 98% RH using D_2O.

mechanism (≤0.4 eV), suggesting that the proton conduction in **TpASH** film follows the proton hopping mechanism.[35] For the **COF-HNU9** film, the activation energy decreased to 0.25 eV and was much lower than 0.4 eV, which was also certainly in the range of a Grotthuss-type mechanism. Considering the hydrophilic property of **COF-HNU9-C**, many water molecules may be involved in the formation of abundant hydrogen-bond networks within the **COF-HNU9** framework after visible light irradiation. This feature explains the unusually high proton conductivity observed above at visible light irradiation and high RH. We also studied the proton conductivity of the **COF-HNU9** film in the environment of D_2O vapor (Fig. 5f). In this case, the proton conductivity of **COF-HNU9** increased from 2.07×10^{-6} to 1.56×10^{-3} S cm^{-1} at 25 °C when the RH was changed from 32% to 98%, which was nearly half smaller than that in a water vapor atmosphere. This result was ascribed to the heavier isotopic effect of D_2O, where the mass of D is twice that of the H atom. As a result, the transport speed of the charge carrier was decreased upon replacing the proton with a deuteron.

In order to investigate the charge transport through the framework, the models with/without water-assisted hydrogen bonds were used to calculate the energy of molecular orbitals (see details in the ESI†). To reduce the computational expense, a dimer structure fragment was built to describe the framework of **COF-HNU9** (Fig. 6). It was shown that in the non-water system (Fig. 6a and b), the HOMO and LUMO were distributed in the two DASA groups, and the charge transport was very difficult due to the large energy difference between the HOMO and LUMO orbitals (about 2.58 eV). In the water-assisted system (Fig. 6c and d), although the HOMO and LUMO distribution was similar with the non-water system, the energy difference of the orbitals was only 1.75 eV, which was significantly less than that in the non-water system. For better illustration of the intermolecular hydrogen bonding shown in Fig. 6, we also modelled the intermolecular hydrogen bonding between water molecules and the small DASA groups without the **COF-HNU9** framework, and calculated the energy of molecular orbitals (Fig. S19†). It was found that the energy difference between the HOMO and LUMO orbitals was 2.69 in the non-water and 2.49 eV in water environment, which was well consistent with the result shown in Fig. 6. It is known that water molecules can form hydrogen bonds and are conducive to the proton or electron transport, so the energy difference was declined in the presence of water vapor. Combined with the experimental results discussed above, these calculation findings suggest that the proton passage in the **COF-HNU9** pores was in the way of proton hopping through the abundant hydrogen-bond networks between water vapor and the closed zwitterionic form of DASA groups inside the **COF-HNU9** framework. Thus, protons can hop through the cavities easily under high RH, while it is almost impossible in a non-water environment.

As a proof of concept, a common electric circuit with LED was assembled to demonstrate the proton conduction change

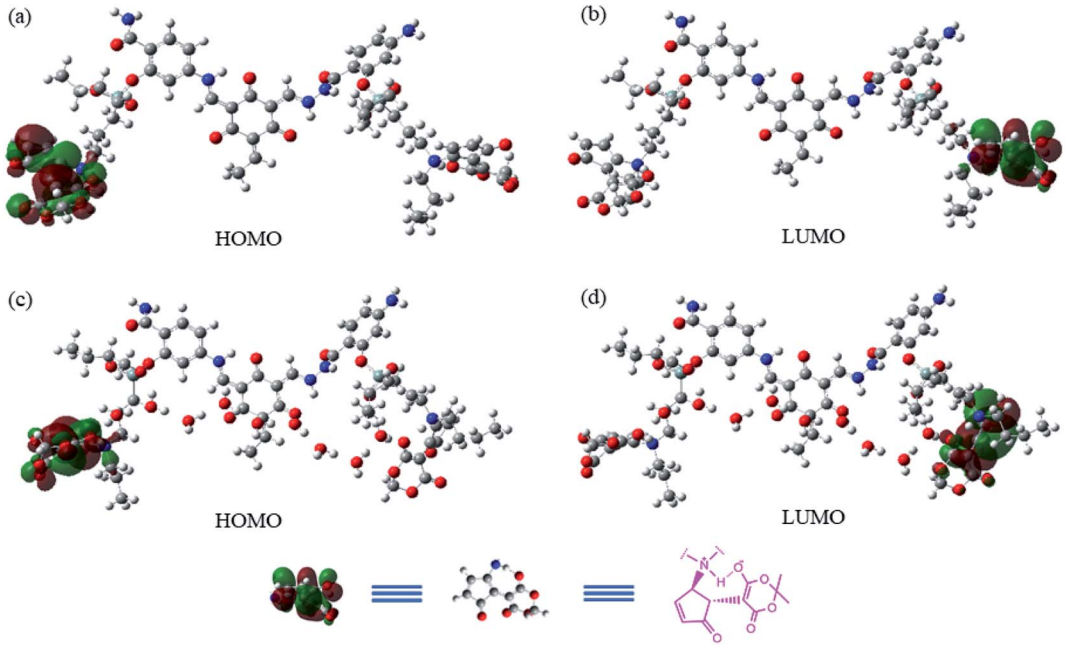

Fig. 6 Frontier molecular orbitals of the structural fragments of COF-HNU9 in non-water (a and b) and water environments (c and d) (C, gray; N, blue; O, red; H, white). A dimer structure fragment is built to describe the COF-HNU9 framework. All geometric structure optimizations were performed at the B3LYP/6-311+G (d, p) level. The calculated energy for HOMO in non-water and water environment was −5.62 and −5.32 eV, and that for the corresponding LUMO was −3.04 and −3.57 eV, respectively.

(Fig. S20 and S21†). Different from the results reported in the recent literature,[20] we built the electric circuit with LED without any amplifier because the current flowing through the circuit was high enough to illuminate the LED lamp under consecutive visible light irradiation. It was found that under 98% RH, the LED lamp was illuminated under the irradiation of visible light at 80 °C, while it was switched off in the dark at 40 °C and 32% RH. This switch on and off process could be operated many times which makes it possible to apply this device under convenient conditions. The key to this photo-controlled process is the remarkable variation in the proton conduction under visible light and in the dark. Before visible light illumination, the film was stored in the dark and existed in its open neutral state (**COF-HNU9-O**), and the resistance was as high as 1.06×10^7 Ω. The current through the lamp was much smaller than the minimum current required to light up the lamp (6 mA). However, after the film was illuminated by visible light at 98% RH and 80 °C, the current through the LED lamp could reach 8 mA without any current amplifier, which was large enough to light up the lamp.

Experimental methods

Synthetic procedures

Synthesis of COF-Glc. COF-Glc was synthesized by the procedures reported in the literature.[36] Briefly, 30 mg of the purified **TpASH** and 1.5 mL of triethylamine were dispersed in 10 mL of absolute ethanol, then sonicated for about 5 min in a water bath. Then 400 μL of glycidol (Glc) was added to the mixture and reacted for 6 h at 80 °C. After the mixture was cooled down, the precipitate was separated, washed with EtOH and dried at 60 °C for 12 h to afford the yellow target COF-Glc.

Synthesis of COF-BAPTMS. COF-BAPTMS was synthesized by following a reported procedure,[37,38] where 50 mg of the as-prepared COF-Glc and 500 μL of (3-butylaminopropyl) trimethoxysilane (BAPTMS) were dispersed in 25 mL of toluene in a N_2 atmosphere. The mixture was refluxed overnight in a N_2 atmosphere, and the product was separated and washed with toluene and EtOH, respectively. Finally, a yellow product was obtained after being dried at 60 °C overnight.

Synthesis of COF-HNU9. 50 mg of the resulting COF-BAPTMS was dispersed in 7 mL of tetrahydrofuran and sonicated for about 5 min in a water bath. Then, to this solution was added 0.6 gram of 5-(furan-2-ylmethylene)-2,2-dimethyl-1,3-dioxane-4,6-dione. The mixture was stirred at room temperature for 20 min and then in ice-water for 10 min. The product was filtered, washed with cold diethyl ether and EtOH, and the brown-colored DASA-modified **COF-HNU9** was obtained after being dried at 80 °C under vacuum.

AC impedance measurements

The conductivity data were determined by impedance spectroscopy using an Autolab CHI600E system. The as-synthesized powder was mechanically pressed into solid pellets, and the measurements were performed by using stainless steel sheets as electrodes. The amplitude of the AC impedance spectrum was 10 mV and the frequency change was in the range of 1 Hz to 1 MHz.

Conclusions

In summary, we grafted photo-switchable DASA groups into the channels of the **TpASH** framework to create the first light/heat responsive **COF-HNU9** film for highly efficient and switchable proton conductivity. It was found that the DASA groups in the nanopores of **COF-HNU9** underwent reversible isomerization from the open neutral isomer to the closed zwitterionic form under the irradiation of visible light at room temperature and reversed back with heating at 40 °C in the dark. The closed zwitterionic isomers significantly improve the proton conductivity through plenty of hydrogen bonds with the water vapor inside the nanochannels. Under visible light illumination, the proton conductivity of **COF-HNU9** film was up to 0.02 S cm^{-1} at 80 °C and 98% RH. Furthermore, this photo-responsive COF allows remarkable photo-modulation of the proton conductivity, and a three orders of magnitude increase was observed. The studies from experimental activation energies and DFT calculations suggest that the proton conduction follows the proton hopping mechanism through the abundant hydrogen bonds between water vapor and the closed zwitterionic form of DASA groups inside the **COF-HNU9** cavities. Furthermore, as an example of the applications of the above findings, an optical control device was assembled by using a light-switching proton conductive **COF-HNU9** film to remotely illuminate an LED lamp and then switch it off without any current amplifier. The findings reported here pave the way toward the development of novel photo-switchable conducting materials based on smart COFs in remote-controllable fuel cells, chemical sensors and other advanced switchable devices. Finally, it should be pointed out that the COF used in this work is asymmetric. In future designs, we will examine whether the asymmetry affects the proton conductivity before and after visible light irradiation.

Data availability

All the data have been included in the ESI.†

Author contributions

J. W. and G. Z. designed the research and proposed the idea. Y. C. conducted the synthesis of the COF films and the performance tests. J. Q. participated in the synthesis. X. Z. performed the DFT calculations. H. W., W. Y., Z. L. and Q. X. participated in the characterizations of BET, FT-IR and XRD of the COF films and the discussion of the manuscript. Y. C. and J. Q. wrote the manuscript. J. W. and G. Z. revised and finalized the manuscript.

Conflicts of interest

There are no conflicts to declare.

Acknowledgements

This work is supported by the National Natural Science Foundation of China (U1704251, 22073024, 21803048), the National Key Research and Development Program of China (2017YFA0403101), the 111 Project (D17007), and the Program for Universities of Henan Province Science & Technology Innovation Talents (21HASTIT003).

Notes and references

1 (*a*) Y. Wang, K. S. Chen, J. Mishler, S. C. Cho and X. C. Adroher, *Appl. Energy*, 2011, **88**, 981–1007; (*b*) M. A. Hickner, H. Ghassemi, Y. S. Kim, B. R. Einsla and J. E. McGrath, *Chem. Rev.*, 2004, **104**, 4587–4612; (*c*) N. L. Garland and J. P. Kopasz, *J. Power Sources*, 2007, **172**, 94–99.

2 (*a*) S. K. Nataraj, C.-H. Wang, H.-C. Huang, H.-Y. Du, S.-F. Wang, Y.-C. Chen, L.-C. Chen and K.-H. Chen, *ChemSusChem*, 2012, **5**, 392–395; (*b*) E. B. Trigg, T. W. Gaines, M. Maréchal, D. E. Moed, P. Rannou, K. B. Wagener, M. J. Stevens and K. I. Winey, *Nat. Mater.*, 2018, **17**, 725–731.

3 (*a*) R.-L. Liu, Y.-R. Liu, S.-H. Yu, C.-L. Yang, Z.-F. Li and G. Li, *ACS Appl. Mater. Interfaces*, 2019, **11**, 1713–1722; (*b*) W. Dou, L. Q. Zhu, J. Jiang and Q. Wan, *Appl. Phys. Lett.*, 2013, **102**, 093509; (*c*) B. Musset, S. M. E. Smith, S. Rajan, D. Morgan, V. V. Cherny and T. E. DeCoursey, *Nature*, 2011, **480**, 273–277; (*d*) M. Yoon, K. Suh, S. Natarajan and K. Kim, *Angew. Chem., Int. Ed.*, 2013, **52**, 2688–2700.

4 (*a*) M. K. Sarango-Ramírez, D.-W. Lim, D. I. Kolokolov, A. E. Khudozhitkov, A. G. Stepanov and H. Kitagawa, *J. Am. Chem. Soc.*, 2020, **142**, 6861–6865; (*b*) Z.-C. Guo, Z.-Q. Shi, X.-Y. Wang, Z.-F. Li and G. Li, *Coord. Chem. Rev.*, 2020, **422**, 213465.

5 (*a*) S. Chand, S. M. Elahi, A. Pal and M. C. Das, *Chem.–Eur. J.*, 2019, **25**, 6259–6269; (*b*) Y. Jiang and L. Heinke, *Langmuir*, 2021, **37**, 2–15.

6 X. Meng, H.-N. Wang, S.-Y. Song and H.-J. Zhang, *Chem. Soc. Rev.*, 2017, **46**, 464–480.

7 D.-W. Lim and H. Kitagawa, *Chem. Rev.*, 2020, **120**, 8416–8467.

8 R.-l. Liu, D.-Y. Wang, J.-R. Shi and G. Li, *Coord. Chem. Rev.*, 2021, **431**, 213747.

9 (*a*) S. Bian, K. Zhang, Y. Wang, Z. Liu, G. Wang, X. Jiang, Y. Pan, B. Xu, G. Huang and G. Zhang, *ACS Appl. Energy Mater.*, 2022, **5**, 1298–1304; (*b*) J. Yang, C. Xie, Q. Yang, S. Wang, Y. Gao, J. Ji, Z. Du, Z. Kang, R. Wang and D. Sun, *Chem. Commun.*, 2022, **58**, 1131–1134.

10 (*a*) Y. Zhai, G. Liu, F. Jin, Y. Zhang, X. Gong, Z. Miao, J. Li, M. Zhang, Y. Cui, L. Zhang, Y. Liu, H. Zhang, Y. Zhao and Y. Zeng, *Angew. Chem., Int. Ed.*, 2019, **58**, 17679–17683; (*b*) Y. Liu, C. S. Diercks, Y. Ma, H. Lyu, C. Zhu, S. A. Alshmimri, S. Alshihri and O. M. Yaghi, *J. Am. Chem. Soc.*, 2019, **141**, 677–683; (*c*) K. Geng, T. He, R. Liu, S. Dalapati, K. T. Tan, Z. Li, S. Tao, Y. Gong, Q. Jiang and D. Jiang, *Chem. Rev.*, 2020, **120**, 8814–8933; (*d*) L. Dai, K. Huang, Y. Xia and Z. Xu, *Green Energy Environ.*, 2021, **6**, 193–211.

11 K. C. Ranjeesh, R. Illathvalappil, S. D. Veer, J. Peter, V. C. Wakchaure, Goudappagouda, K. V. Raj, S. Kurungot and S. S. Babu, *J. Am. Chem. Soc.*, 2019, **141**, 14950–14954.
12 Y. Peng, G. Xu, Z. Hu, Y. Cheng, C. Chi, D. Yuan, H. Cheng and D. Zhao, *ACS Appl. Mater. Interfaces*, 2016, **8**, 18505–18512.
13 S. Chandra, T. Kundu, K. Dey, M. Addicoat, T. Heine and R. Banerjee, *Chem. Mater.*, 2016, **28**, 1489–1494.
14 L. Cao, H. Wu, Y. Cao, C. Fan, R. Zhao, X. He, P. Yang, B. Shi, X. You and Z. Jiang, *Adv. Mater.*, 2020, **32**, 2005565.
15 (*a*) S. Chandra, T. Kundu, S. Kandambeth, R. BabaRao, Y. Marathe, S. M. Kunjir and R. Banerjee, *J. Am. Chem. Soc.*, 2014, **136**, 6570–6573; (*b*) Z. Meng, A. Aykanat and K. A. Mirica, *Chem. Mater.*, 2019, **31**, 819–825; (*c*) Y. Yang, X. He, P. Zhang, Y. H. Andaloussi, H. Zhang, Z. Jiang, Y. Chen, S. Ma, P. Cheng and Z. Zhang, *Angew. Chem., Int. Ed.*, 2020, **59**, 3678–3684.
16 (*a*) H. Ma, B. Liu, B. Li, L. Zhang, Y.-G. Li, H.-Q. Tan, H.-Y. Zang and G. Zhu, *J. Am. Chem. Soc.*, 2016, **138**, 5897–5903; (*b*) L. Liu, L. Yin, D. Cheng, S. Zhao, H.-Y. Zang, N. Zhang and G. Zhu, *Angew. Chem., Int. Ed.*, 2021, **60**, 14875–14880.
17 (*a*) S. Tao, L. Zhai, A. D. D. Wonanke, M. A. Addicoat, Q. Jiang and D. Jiang, *Nat. Commun.*, 2020, **11**, 1981; (*b*) J. Li, J. Wang, Z. Wu, S. Tao and D. Jiang, *Angew. Chem., Int. Ed.*, 2021, **60**, 12918–12923; (*c*) X. Wu, Y.-L. Hong, B. Xu, Y. Nishiyama, W. Jiang, J. Zhu, G. Zhang, S. Kitagawa and S. Horike, *J. Am. Chem. Soc.*, 2020, **142**, 14357–14364.
18 (*a*) H. S. Sasmal, H. B. Aiyappa, S. N. Bhange, S. Karak, A. Halder, S. Kurungot and R. Banerjee, *Angew. Chem., Int. Ed.*, 2018, **57**, 10894–10898; (*b*) Y. Li, H. Wu, Y. Yin, L. Cao, X. He, B. Shi, J. Li, M. Xu and Z. Jiang, *J. Membr. Sci.*, 2018, **568**, 1–9.
19 S. Li, Y. Liu, L. Li, C. Liu, J. Li, S. Ashraf, P. Li and B. Wang, *ACS Appl. Mater. Interfaces*, 2020, **12**, 22910–22916.
20 H.-Q. Liang, Y. Guo, Y. Shi, X. Peng, B. Liang and B. Chen, *Angew. Chem., Int. Ed.*, 2020, **59**, 7732–7737.
21 (*a*) S. S. Nagarkar, S. Horike, T. Itakura, B. L. Ouay, A. Demessence, M. Tsujimoto and S. Kitagawa, *Angew. Chem., Int. Ed.*, 2017, **56**, 4976–4981; (*b*) K. Müller, J. Helfferich, F. Zhao, R. Verma, A. B. Kanj, V. Meded, D. Bléger, W. Wenzel and L. Heinke, *Adv. Mater.*, 2018, **30**, 1706551; (*c*) A. B. Kanj, A. Chandresh, A. Gerwien, S. Grosjean, S. Bräse, Y. Wang, H. Dube and L. Heinke, *Chem. Sci.*, 2020, **11**, 1404–1410.
22 (*a*) N. Huang, X. Ding, J. Kim, H. Ihee and D. Jiang, *Angew. Chem., Int. Ed.*, 2015, **54**, 8704–8707; (*b*) P. She, Y. Qin, X. Wang and Q. Zhang, *Adv. Mater.*, 2021, 2101175; (*c*) S. Jhulki, A. M. Evans, X.-L. Hao, M. W. Cooper, C. H. Feriante, J. Leisen, H. Li, D. Lam, M. C. Hersam, S. Barlow, J.-L. Brédas, W. R. Dichtel and S. R. Marder, *J. Am. Chem. Soc.*, 2020, **142**, 783–791.
23 R. Ou, H. Zhang, V. X. Truong, L. Zhang, H. M. Hegab, L. Han, J. Hou, X. Zhang, A. Deletic, L. Jiang, G. P. Simon and H. Wang, *Nat. Sustain.*, 2020, **3**, 1052–1058.
24 (*a*) Y. Chen, Z. Li, H. Wang, Y. Pei, Y. Shi and J. Wang, *Langmuir*, 2018, **34**, 2784–2790; (*b*) Z. Li, Y. Feng, X. Liu, H. Wang, Y. Pei, H. Q. Nimal Gunaratne and J. Wang, *ACS Sustainable Chem. Eng.*, 2020, **8**, 15327–15335.
25 (*a*) E. A. Dolgopolova, V. A. Galitskiy, C. R. Martin, H. N. Gregory, B. J. Yarbrough, A. M. Rice, A. A. Berseneva, O. A. Ejegbavwo, K. S. Stephenson, P. Kittikhunnatham, S. G. Karakalos, M. D. Smith, A. B. Greytak, S. Garashchuk and N. B. Shustova, *J. Am. Chem. Soc.*, 2019, **141**, 5350–5358; (*b*) F. Yu, W. Liu, B. Li, D. Tian, J.-L. Zuo and Q. Zhang, *Angew. Chem., Int. Ed.*, 2019, **58**, 16101–16104; (*c*) K. Griffiths, N. R. Halcovitch and J. M. Griffin, *Chem. Sci.*, 2022, **13**, 3014–3019; (*d*) C. Liu, W. Zhang, Q. Zeng and S. Lei, *Chem.–Eur. J.*, 2016, **22**, 6768–6773.
26 (*a*) S. Helmy, F. A. Leibfarth, S. Oh, J. E. Poelma, C. J. Hawker and J. Read de Alaniz, *J. Am. Chem. Soc.*, 2014, **136**, 8169–8172; (*b*) T. Senthilkumar, L. Zhou, Q. Gu, L. Liu, F. Lv and S. Wang, *Angew. Chem., Int. Ed.*, 2018, **57**, 13114–13119.
27 S. Mitra, H. S. Sasmal, T. Kundu, S. Kandambeth, K. Illath, D. Díaz Díaz and R. Banerjee, *J. Am. Chem. Soc.*, 2017, **139**, 4513–4520.
28 N. Mallo, E. D. Foley, H. Iranmanesh, A. D. W. Kennedy, E. T. Luis, J. Ho, J. B. Harper and J. E. Beves, *Chem. Sci.*, 2018, **9**, 8242–8252.
29 (*a*) W.-R. Cui, C.-R. Zhang, W. Jiang, R.-P. Liang and J.-D. Qiu, *ACS Appl. Nano Mater.*, 2019, **2**, 5342–5349; (*b*) R. Khatuna, S. Biswasa, I. H. Biswasa, S. Riyajuddinb, N. Haquea, K. Ghoshb and S. M. Islama, *J. CO2 Util.*, 2020, **40**, 101180.
30 T.-T. Liu, R. Xu, J.-D. Yi, J. Liang, X.-S. Wang, P.-C. Shi, Y.-B. Huang and R. Cao, *ChemCatChem*, 2018, **10**, 2036–2040.
31 G. Das, T. Prakasam, M. A. Addicoat, S. K. Sharma, F. Ravaux, R. Mathew, M. Baias, R. Jagannathan, M. A. Olson and A. Trabolsi, *J. Am. Chem. Soc.*, 2019, **141**, 19078–19087.
32 S. Helmy, S. Oh, F. A. Leibfarth, C. J. Hawker and J. Read de Alaniz, *J. Org. Chem.*, 2014, **79**, 11316–11329.
33 H. Farahani, R. Wagiran and G. A. Urban, *IEEE Sens. J.*, 2021, **21**, 9657–9666.
34 G. Zhang and D. M. Smyth, *Solid State Ionics*, 1995, **82**, 153–160.
35 (*a*) N. Agmon, *Chem. Phys. Lett.*, 1995, **244**, 456–462; (*b*) K.-D. Kreuer, *Chem. Mater.*, 1996, **8**, 610–641.
36 J. Chen and W. Shum, *Tetrahedron Lett.*, 1995, **36**, 2379–2380.
37 S. Mitra, B. Subia, P. Patra, S. Chandra, N. Debnath, S. Das, R. Banerjee, S. C. Kundu, P. Pramanik and A. Goswami, *J. Mater. Chem.*, 2012, **22**, 24145–24154.
38 Y. Guo, H. Wang, C. He, L. Qiu and X. Cao, *Langmuir*, 2009, **25**, 4678–4684.